ARTICLE

Chinese Journal of Structural Chemistry

$NiSe_2$-$CoSe_2$ with a Hybrid Nanorods and Nanoparticles Structure for Efficient Oxygen Evolution Reaction

Meng Li[1] and Ligang Feng[1]*

[1]*School of Chemistry and Chemical Engineering, Yangzhou University, Yangzhou 225002, China*

ABSTRACT Hetero-structure induced high performance catalyst for oxygen evolution reaction (OER) in the water splitting reaction has received increased attention. Herein, we demonstrated a novel catalyst system of $NiSe_2$-$CoSe_2$ consisting of nanorods and nanoparticles for the efficient OER in the alkaline electrolyte. This catalyst system can be easily fabricated via a low-temperature selenization of the solvothermal synthesized $NiCo(OH)_x$ precursor and the unique morphology of hybrid nanorods and nanoparticles was found by the electron microscopy analysis. The high valence state of the metal species was indicated by X-ray photoelectron spectroscopy study and a strong electronic effect was found in the $NiSe_2$-$CoSe_2$ catalyst system compared to their counterparts. As a result, $NiSe_2$-$CoSe_2$ exhibited high catalytic performance with a low overpotential of 250 mV to reach 10 $mA{\cdot}cm^{-2}$ for OER in the alkaline solution. Furthermore, high catalytic stability and catalytic kinetics were also observed. The superior performance can be attributed to the high valence states of Ni and Co and their strong synergetic coupling effect between the nanorods and nanoparticles, which could accelerate the charge transfer and offer abundant electrocatalytic active sites. The current work offers an efficient hetero-structure catalyst system for OER, and the results are helpful for the catalysis understanding.

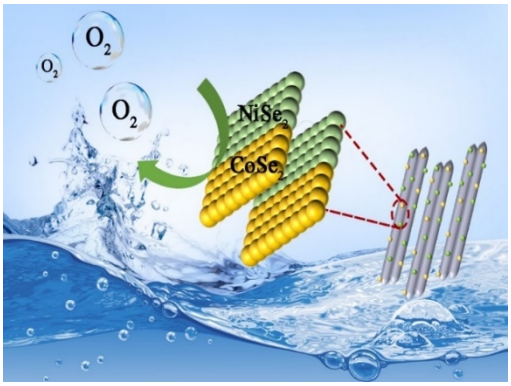

Keywords: oxygen evolution reaction, $NiSe_2$, $CoSe_2$, hetero-structure, electrocatalysis

n INTRODUNTION

The rapid depletion of fossil fuels and their associated global climate change urgently require clean energies for energy storage and conversion devices.[1-3] While the intermittent nature of the clean energy of solar energy and wind energy etc. is impossible to realize the continuous application, transferring these energies to the chemical energy of hydrogen for storage via water splitting reaction is an attractive method to compensate for the intermittence character.[4-8] Oxygen evolution reaction (OER) is much more sluggish in kinetics as it requires a four-electron transfer process compared to the cathode hydrogen evolution reaction.[9,10] OER happens at a relatively high overpotential without the help of electrocatalysts, resulting in low efficiency and the waste of energy.[11-13] Therefore, efficient catalysts that could facilitate multiple electrons and proton coupling process under low over-potential are highly desired.[14,15] In light of the high cost and rareness of noble metal-based catalyst, the attention is directed to earth-abundant first-row transition metal-based catalysts.[16-18]

Among various alternative materials, the transition metal chalcogenides have attracted a great deal of attention due to their unique *d*-orbital electron configuration and high corrosion resistance in alkaline electrolyte solutions.[19,20] The 3*d* orbital of Se can bond with metal atoms due to its close energy level to that of 3*s* and 3*p* orbitals for the transition metals.[21] Therefore, metal selenides possess greater metallicity compared to the transition metal oxides and sulfides that benefit the electron transfer for reactions.[22,23] Hence, transition metal selenides are regarded as one type of the most promising electrocatalysts for OER.[24,25] Note that most of the mono-metal selenides have modest catalytic performance due to the single active site and insufficient electronic structure synergism. The bimetallic selenides catalysts thus have been developed to overcome these problems, and largely improved catalytic ability is reported resulting from the increased active sites, efficient electronic effect and structural synergism. For example, a three-dimensional Ni-Co selenide ($NiCoSe_2$) nanonetwork was prepared for the OER, and a low overpotential of 274 mV was required to reach 10 $mA{\cdot}cm^{-2}$ with excellent stability.[26] Furthermore, the catalytic performance can be enhanced by the synergistic effect of hetero-atomic doping and interface engineering due to electronic interactions and ligand effects between the different active components.[5,27] The in situ formed $NiSe/NiO_x$ core/shell nanostructure from NiSe under electrocatalytic conditions showed a current density of 10 $mA{\cdot}cm^{-2}$ at a low overpotential of ~243 mV.[28] A hybrid catalyst system of $NiSe_2$ nanoparticle/NiO nanosheet demonstrated an efficient synergism for urea-assisted water electrolysis reactions.[29] The high performance was attributed to the efficient coupling effect between $NiSe_2$ and NiO, and the increased Ni^{3+} ions. The $CoSe_2$@$NiSe_2$ materials grown on nickel foam exhibited high efficiency of water splitting reaction due to high electro-chemically active surface area and synergistic effect.[30] Ultrathin dual-phase $CoSe_2$-$NiSe_2$/CN nanosheets were reported highly efficient and stable for the HER resulting from the ultrathin nanostructure and biphasic synergy.[31] Therefore, the catalytic performance of bimetallic selenides could be boosted by chemical composition adjustment and nanostructure engineering.

Hence, we demonstrated a new hybrid catalyst of $NiSe_2$-$CoSe_2$ in the form of nanoparticles/nanorods as an efficient and stable electrocatalyst for oxygen evolution reaction. Due to its fast

DOI: 10.14102/j.cnki.0254-5861.2021-0037

electron transfer rate, increased content of high-valence state metal species, the synergy between Ni/Co atoms and the hybrid structure of nanoparticles/nanorods connected, the $NiSe_2$-$CoSe_2$ composite catalyst exhibited good catalytic activity and durability for OER. Specifically, a low overpotential of 250 mV was required to reach a current density of 10 mA·cm^{-2} for OER when supported over the inert glass carbon electrode. In addition, it also showed excellent long-term stability and efficient catalytic kinetics.

n RESULTS AND DISCUSSION

The synthesis process of $NiSe_2$-$CoSe_2$ catalyst was systematically described in Scheme 1 including the solvothermal reaction for $NiCo(OH)_x$ precursor fabrication and the subsequent selenization process. Briefly, the nanorod-shaped $NiCo(OH)_x$ precursor with a small number of nanoparticles was prepared firstly, and then, the precursor was selenized using the selenium powder under N_2 atmosphere at 350 °C to get the $NiSe_2$-$CoSe_2$ sample (details see the supporting information). The crystalline structure of the as-prepared catalyst was probed by the powder X-ray diffraction technique (XRD). No obvious diffraction peaks were observed for the precursors of $NiCo(OH)_x$, while, after selenization, very strong diffraction peaks were observed in the XRD patterns (Figure 1a). Interestingly, these characteristic peaks were located in the middle of the standard characteristic peaks of $NiSe_2$ (PDF No. 41-1495) and $CoSe_2$ (PDF No. 09-0234) due to the hybridization of Ni and Co in the system. These characteristic peaks indicated the successful preparation of $NiSe_2$-$CoSe_2$ catalyst with the pyrite cubic phase.

The surface chemical state of the $NiSe_2$-$CoSe_2$ was probed by X-ray photoelectron spectroscopy (XPS) measurements compared to the $NiSe_2$ and $CoSe_2$ alone. The whole spectrum survey showed the presence of the concerned elements, and the binging energy was calibrated by the main peak of C 1*s* at 284.8 eV (Figure S1). The high-resolution spectrum of Ni 2*p* consists of two components, namely $2p_{1/2}$ and $2p_{3/2}$, respectively, and each component can be deconvoluted into Ni–Se (Ni^{2+}), Ni–O (Ni^{3+}) bond and the accompanied satellite peaks, respectively (Table S1).[29] Specifically, the peak position of Ni–Se locates at 853.8 and 871.1 eV in the $2p_{1/2}$ and $2p_{3/2}$ for $NiSe_2$-$CoSe_2$; and these peaks are shifted to the high binding energy direction by 0.7 eV compared to that of the $NiSe_2$ alone due to the chemical environment change for the hybrid $NiSe_2$-$CoSe_2$. Note that the Ni^{3+} dominates the contents of Ni in the $NiSe_2$-$CoSe_2$ (55%), and the ratio of the content for Ni^{3+}/Ni^{2+} is 1.22, much higher than that of 0.69 for the $NiSe_2$ catalyst. Therefore, more content of high valence state Ni^{3+} is formed in the sample of $NiSe_2$-$CoSe_2$, which can provide more active sites for the oxygen evolution reaction and accelerate the oxygen evolution reaction rate because the high valence state of Ni species is proposed as the real active phase.[32] The narrow spectrum of Co 2*p* has two spin orbitals of Co $2p_{1/2}$ and Co $2p_{3/2}$, respectively and each band can be deconvoluted into different chemical states by four peaks, namely the metallic Co (Co–Se), Co^{3+}, Co^{2+} and satellite peaks (Table S2). It is noticed the profiles of the Co 2*p* spectrum are different indicating the varied content of the different chemical states. Specifically, the peak position of Co–Se locates at 778.2 eV; and the surface oxidized Co is indicated by the peaks of Co^{3+} at 780.0 eV and Co^{2+} at 781.6 eV for $2p_{3/2}$, respectively.[33] These peak positions are shifted to the low binding energy direction by 0.4 eV compared to that of the pure $CoSe_2$ catalyst, echoing with the positive shift of the binding energy observed for the Ni species. Furthermore, the metallic Co as Co–Se accounts for 42% of the content for $CoSe_2$ catalyst alone, while the content is reduced in the $NiSe_2$-$CoSe_2$ sample (19.3%), where the oxidized state of Co dominates the surface content (Table S2). Moreover, the content of high valence state of Co^{3+} was also found much higher in the $NiSe_2$-$CoSe_2$ system (43.4%). For the spectrum of Se 3*d*, the peaks of Se–O and Se-metal bonds are observed (Figure 1d). The peak at 58.8 eV is assigned to SeO_x species formed on the surface, and the other two peaks fitted at 54.1 and 55.0 eV are assigned to the chemical bonds of Se-metal. The formation of $NiSe_2$-$CoSe_2$ might be much easier for the high valence state of metal oxide species generation than their counterparts alone as indicated by the above XPS results. The more content of high valent metal species in the $NiSe_2$-$CoSe_2$ would contribute to the active phase formation and thereby promote the OER performance.[32,34]

The morphology of $NiCo(OH)_x$ precursor was probed by scanning electron microscopy (SEM), and the hybrid morphology of nanoparticels and nanorods was observed (Figure S2a). After selenizaiton, the obtained $NiSe_2$-$CoSe_2$ showed similar morphology with the nanoparticles anchored on the nanorods in-

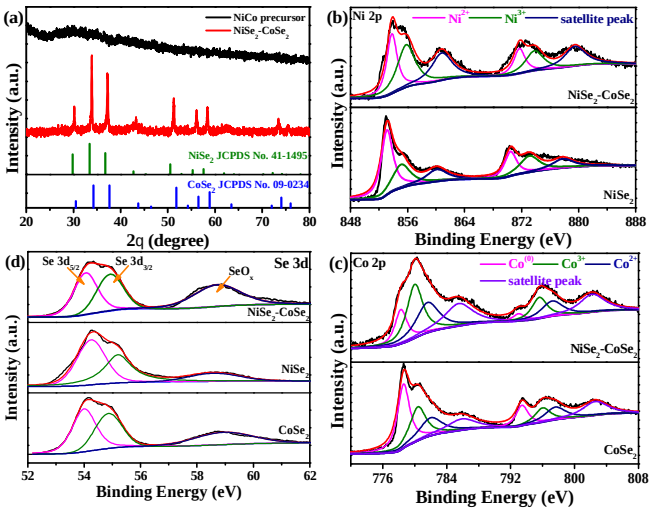

Figure 1. XRD pattern of $NiSe_2$-$CoSe_2$ (a). High-resolution XPS spectra of Ni 2*p* (b), Co 2*p* (c) and Se 3*d* (d) for $NiSe_2$-$CoSe_2$, $NiSe_2$ and $CoSe_2$.

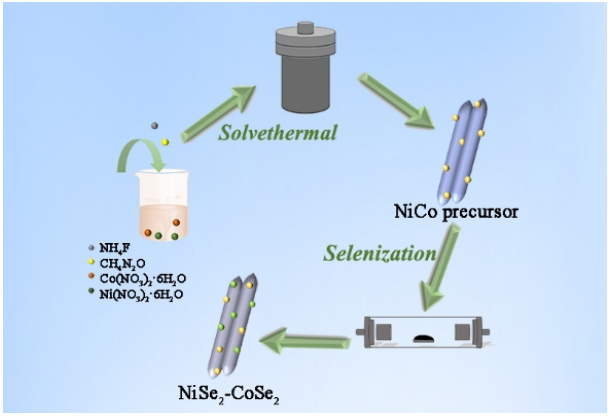

Scheme 1. Schematic illustration of the preparation of $NiSe_2$-$CoSe_2$.

DOI: 10.14102/j.cnki.0254-5861.2021-0037

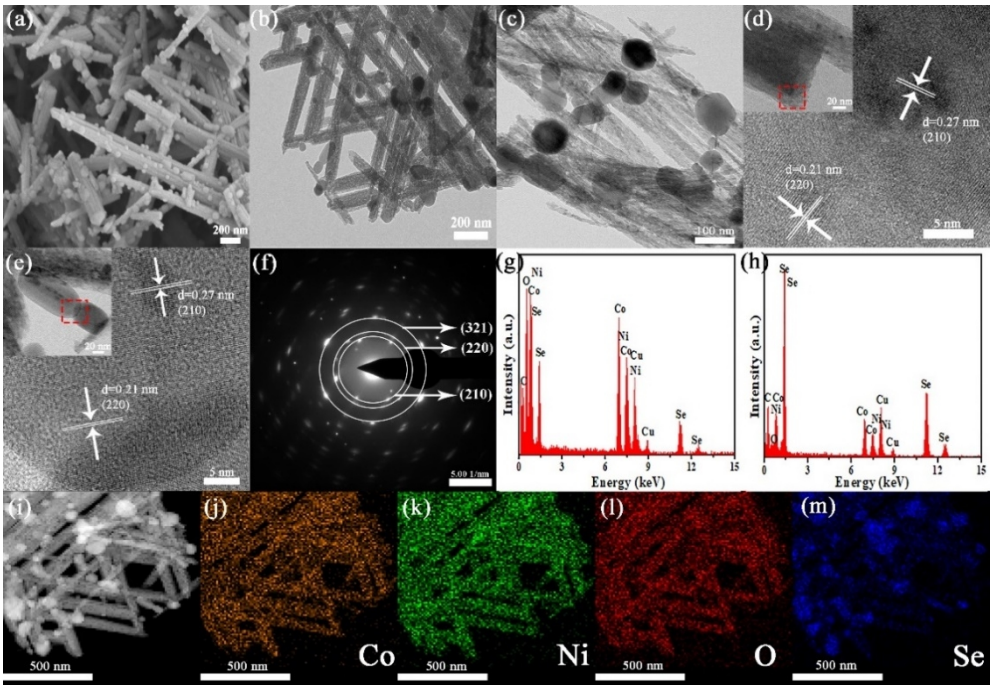

Figure 2. SEM (a), TEM (b–c), HRTEM image of nanorod and inset of local TEM image (d), HRTEM image of nanoparticle and inset of local TEM image (e), SAED pattern (f), corresponding EDX spectrum for nanorod (g) and nanoparticle (h), the corresponding STEM and elemental mapping images of $NiSe_2$-$CoSe_2$ (i–m).

creased (Figure 2a). The local morphology and microstructure of $NiSe_2$-$CoSe_2$ were further observed by transmission electron microscopy (TEM). The nanorods were cross-linked and some nanoparticles were anchored over the nanorods (Figure 2b–c). The local nanorods (Figure 2d) and particles (Figure 2e) were further observed by TEM and high-resolution TEM (HRTEM), and the crystalline interplanar spacings of 0.21 and 0.27 nm assigned to the (220) and (210) crystal faces were indicated for the cubic structures of $NiSe_2$ and $CoSe_2$ (Figure S2b). Some strong diffraction spots were observed in the selected area electron diffraction (SAED) pattern (Figure 2f). The contents of the concerned elements of Ni, Co, Se and O in the nanorods and nanoparticles were probed by energy dispersion X-ray spectroscopy (EDX) (Figure 2g–h). Interestingly, the contents of elements were different in the nanorods and the nanoparticles (Table S3 and S4). There was more Se in the nanoparticles than that in the nanorods probably because of the easy surface oxidation of the nanorods. This could be further confirmed by the element mapping images, where Ni and Co were uniformly distributed over nanorods and nanoparticles, and the distribution of O was accompanied with the metals but Se was mainly concentrated in the nanoparticles (Figure 2i–m); This result was in line with the results of EDX analysis. Therefore, $NiSe_2$-$CoSe_2$ with the hybrid structure of nanoparticles and nanorods was obtained by a simple selenization reaction for the $NiCo(OH)_x$ precursor. These interconnected nanorods and nanoparticles could expose more active sites and promote mass transfer, which would be beneficial to the following electrochemical reactions.

The as-prepared powder catalysts of $NiSe_2$-$CoSe_2$, $NiSe_2$ and $CoSe_2$ were compared for the oxygen evolution in a conventional three-electrode system loaded on a glassy carbon electrode in N_2-saturated 1 M KOH solution with a scan rate of 5 $mV{\cdot}s^{-1}$. The benchmark current density of 10 $mA{\cdot}cm^{-2}$ on the inert electrode was employed to evaluate the catalytic performance and all polarization curves were shown with IR-correction by the positive feedback of compensating 80% of the uncompensated solution resistance. As anticipated, $NiSe_2$-$CoSe_2$ exhibits much higher OER activity than $NiSe_2$ and $CoSe_2$. Specifically, $NiSe_2$-$CoSe_2$ requires an overpotential of 250 mV to afford 10 $mA{\cdot}cm^{-2}$, while to reach the same current density, $NiSe_2$ and $CoSe_2$ need the overpotential of 339 and 338 mV, respectively (Figure 3a). This performance is also much better than that of a commercial IrO_2 catalyst (ca. 310 mV) and some similar work recently reported (Table S5). The Tafel slope was analyzed to probe the catalytic kinetics based on the catalytic mechanism in the kinetic range. The Tafel slope was measured to be 49.3 $mV{\cdot}dec^{-1}$, which is much smaller than that of $NiSe_2$ (66.7 $mV{\cdot}dec^{-1}$) and $CoSe_2$ (56.1 $mV{\cdot}dec^{-1}$). The Tafel slope with a value around 60 $mV{\cdot}dec^{-1}$ indicates the rate-determining step of M–O generation from the M–OH.[35] Here, $NiSe_2$-$CoSe_2$ has a much smaller value, indicating the much faster catalytic kinetics. This can be further verified by the charge transfer ability as revealed by the electrochemical impedance spectroscopy shown in Figure 3c. The semi-circle or arc of $NiSe_2$-$CoSe_2$ is much smaller than that of $NiSe_2$ and $CoSe_2$, signifying the greatly improved charge transfer ability and catalytic kinetics in the OER process (Figure 3c). To be specific, the charge transfer resistance (R_{ct}) value can be obtained by fitting the Nyquist plots using an equivalent circuit (Figure S3 and Table S6). The value was fitted to be 44.4 Ω for $NiSe_2$-$CoSe_2$ catalyst, remarkably smaller than that of $NiSe_2$ (362.6 Ω) and $CoSe_2$ (284.1 Ω). The largely improved catalytic kinetics should be due to the synergistic effect of Ni and Co as indicated by the above analysis.[36]

In order to investigate the catalytic efficiency of the catalyst for OER, the electrochemical surface area (ECSA) of the catalyst was calculated by the electrochemical double-layer capacitance

DOI: 10.14102/j.cnki.0254-5861.2021-0037

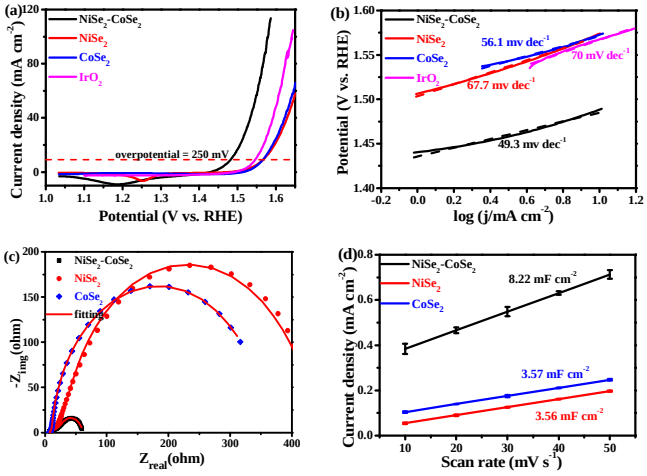

Figure 3. Polarization curves (a), Tafel slope of $NiSe_2$-$CoSe_2$, $NiSe_2$, $CoSe_2$ and IrO_2 (b). Nyquist plots (c), scan-rate dependence of the current densities derived from double-layer capacitance measurements (d) for $NiSe_2$-$CoSe_2$, $NiSe_2$, $CoSe_2$.

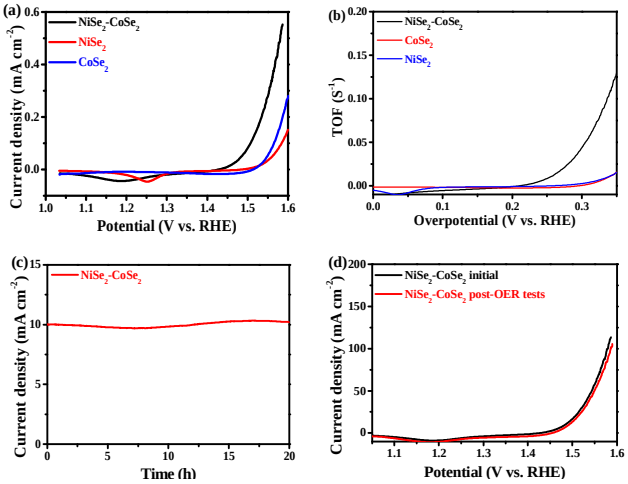

Figure 4. Polarization curve for the specific activity (a) and TOF value (b) of $NiSe_2$-$CoSe_2$, $NiSe_2$, $CoSe_2$. CA curves at 1.48 V vs. RHE (c) and polarization curves before and after 1000 CV cycles of $NiSe_2$-$CoSe_2$ in 1 M KOH (d).

(C_{dl}) approach. The value of C_{dl} for $NiSe_2$-$CoSe_2$ is 8.22 mF·cm^{-2}, which is much larger than that of 3.56 mF·cm^{-2} for $NiSe_2$ and 3.57 mF·cm^{-2} for $CoSe_2$ (Figure 3d and Figure S4). The ECSA was calculated by normalizing the C_{dl} (in mF) to a standard specific capacitance for a flat surface of 0.040 mF·cm^{-2} according to previous literature.[37,38] The ECSA of $NiSe_2$-$CoSe_2$ was calculated to be 14.39 cm^{-2}, which was approximately 2.31 times that of $NiSe_2$ and $CoSe_2$ (Table S7). The surface roughness factor (R_f) was calculated by normalizing the ECSA to the geometric surface area of the electrode, and the largest R_f value of 205.5 was found on $NiSe_2$-$CoSe_2$ catalyst, indicating the largely increased surface roughness for the hybrid $NiSe_2$-$CoSe_2$ catalyst.

In order to compare the catalytic efficiency of the active sites, the specific activity was compared for these catalysts by normalizing the current to the ECSA (Figure 4a). Obviously, the specific activity of $NiSe_2$-$CoSe_2$ catalyst was much higher than that of the other two catalysts. For example, the specific current density of $NiSe_2$-$CoSe_2$ at the overpotential of 350 mV was 0.49 mA·cm^{-2}, ca. 5.4 times of $NiSe_2$ and 3.1 times of $CoSe_2$. A similar order to that of the specific activity was found on turnover frequency (TOF) polarization curves, which can be relatively fair to evaluate the intrinsic activity (Figure 4b). The TOF value of $NiSe_2$-$CoSe_2$ reaches 0.131 s^{-1} at the overpotential of 350 mV, which is 8.73 and 8.12 times higher than those of $NiSe_2$ (0.015 s^{-1}) and $CoSe_2$ (0.016 s^{-1}), respectively. The higher TOF values indicate the formation of the hybrid structure of NiSe-CoSe could largely increase the intrinsic activity for OER. Finally, the electrochemical stability was evaluated on the $NiSe_2$-$CoSe_2$ catalyst to probe the stability for long-term operation. The consecutive cyclic voltammetry (CV) and chronoamperometry techniques were performed to investigate the catalytic stability of $NiSe_2$-$CoSe_2$ for OER. The chronoamperometry was conducted for 20 hours at the potential of 1.48 V vs. RHE, and good catalytic stability was observed during the operation for 20 hours (Figure 4c). The consecutive CV was measured for 1 000 CV cycles at an accelerated stability test and the polarization curves before and after the test were compared (Figure 4d). These polarization curves were very close and the overpotential of only ca. 10 mV was incurred to reach the current of 10 mA·cm^{-2} for OER, indicating good catalytic stability for the dynamic measurement (Figure 4d). Moreover, the morphology of the catalyst after the stability was well maintained indicates a good physical stability during the catalysis (Figure S5).

From the above results, it can be concluded that the as-prepared $NiSe_2$-$CoSe_2$ catalyst exhibited high catalytic performance for OER. Though the transition metal selenide was reported to have good catalytic performance for OER, the single metal-based catalyst showed much lower performance due to the insufficient active site and low intrinsic activity. By forming the hybrid structure of $NiSe_2$-$CoSe_2$, due to the synergistic effect of the different components, the strong electronic effect and the high amount of high valence state metal species generated, and the catalytic performance can be largely improved as seen in the above electrochemical measurements. The high oxidation states of Ni and Co are both active substances in the catalyst, which can effectively help accelerate multi-electron transfer and promote OH^- adsorption and reaction.[39] As reported in the literature, Ni species as the active sites for OER can promote the formation of M=O with the help of high valence state Co^{3+} species as confirmed by the Tafel slope value, and the subsequent O_2 generation from the M-O-O intermediates.[40] Therefore, an accelerated OER kinetics was observed. Besides, the increased catalytic efficiency of the active sites was also confirmed by the specific activity and the TOF values, indicating the intrinsic activity boosting by forming the synergistic $NiSe_2$-$CoSe_2$ catalyst, though the hybrid nanostructure possessed a large surface area and high active site exposure.

n CONCLUSION

In summary, a novel catalyst system of hybrid $NiSe_2$-$CoSe_2$ was demonstrated as a high-performing catalyst for OER in the water splitting reaction. An interconnected hybrid structure of nanorods/nanoparticles was demonstrated by spectral study and microscopic analysis. In light of the increased amount of high valence state metal species, the coupling effect between nanorods and nanoparticles, and the strong electronic effect of Ni and

DOI: 10.14102/j.cnki.0254-5861.2021-0037

Co elements, outstanding catalytic performances of high catalytic activity, stability and fast reaction kinetics were observed on $NiSe_2$-$CoSe_2$ for water oxidation compared to their counterparts. Specifically, $NiSe_2$-$CoSe_2$ catalyst exhibited the catalytic performance of 10 $mA \cdot cm^{-2}$ with a low overpotential of 250 mV when loaded on the glassy carbon electrode, outperforming the individual component of $NiSe_2$ and $CoSe_2$ catalysts as well as the similar catalysts. The current results are helpful for the efficient heterostructured catalyst design and fabrication as well as their understanding of the catalysis reaction.

n ACKNOWLEDGEMENTS

The work is supported by the National Natural Science Foundation of China (21972124), the Priority Academic Program Development of Jiangsu Higher Education Institution. L Feng also appreciates the support of the Six Talent Peaks Project of Jiangsu Province (XCL-070-2018). We also thank the experimental assistance from Chengzhe Zhang.

n AUTHOR INFORMATION

Corresponding authors. Email: ligang.feng@yzu.edu.cn, fenglg11@gmail.com (L Feng*)

n COMPETING INTERESTS

The authors declare no competing interests.

n ADDITIONAL INFORMATION

Supplementary information is available for this paper at http://manu30.magtech.com.cn/jghx/EN/10.14102/j.cnki.0254-5861.2021-0037

For submission: https://mc03.manuscriptcentral.com/cjsc

n REFERENCES

(1) Kim, H. Y.; Joo, S. H. Recent advances in nanostructured intermetallic electrocatalysts for renewable energy conversion reactions. *J. Mater. Chem. A* **2020**, 8, 8195–8217.

(2) Fang, B.; Feng, L. PtCo-NC catalyst derived from the pyrolysis of Pt-incorporated ZIF-67 for alcohols fuel electrooxidation. *Acta Phys. -Chim. Sin.* **2020**, 36, 1905023.

(3) Zhang, W.; Ma, X.; Zou, S.; Cai, W. Recent advances in glycerol electrooxidation on Pt and Pd: from reaction mechanisms to catalytic materials, *J. Electrochem.* **2021**, 27, 233–256.

(4) Jing, H.; Zhu, P.; Zheng, X.; Zhang, Z.; Wang, D.; Li, Y. Theory-oriented screening and discovery of advanced energy transformation materials in electrocatalysis. *Adv. Powder Mater.* **2021**, https://doi.org/10.1016/j.apmate.2021.10.004.

(5) Fang, B.; Liu, Z.; Bao, Y.; Feng, L. Unstable Ni leaching in MOF-derived PtNi-C catalyst with improved performance for alcohols fuel electro-oxidation. *Chin. Chem. Lett.* **2020**, 31, 2259–2262.

(6) Wang, Z.; Fan, J.; Cheng, B.; Yu, J.; Xu, J. Nickel-based cocatalysts for photocatalysis: hydrogen evolution, overall water splitting and CO_2 reduction. *Mater. Today Phys.* **2020**, 15, 100279.

(7) Sun, H.; Zhang, W.; Li, J.; Li, Z.; Ao, X.; Xue, K.; Ostrikov, K. K.; Tang, J.; Wang, C. Rh-engineered ultrathin NiFe-LDH nanosheets enable highly-efficient overall water splitting and urea electrolysis. *Appl. Catal., B* **2021**, 284, 119740.

(8) Sun, H.; Yang, J.; Li, J.; Li, Z.; Ao, X.; Liu, Y.; Zhang, Y.; Li, Y.; Wang, C.; Tang, J. Synergistic coupling of NiTe nanoarrays with RuO_2 and NiFe-LDH layers for high-efficiency electrochemical-/photovoltage-driven overall water splitting. *Appl. Catal., B* **2020**, 272, 118988.

(9) Jiao, Y.; Zheng, Y.; Jaroniec, M.; Qiao, S. Z. Design of electrocatalysts for oxygen- and hydrogen-involving energy conversion reactions. *Chem. Soc. Rev.* **2015**, 44, 2060–2086.

(10) Zhao, Y.; Nakamura, R.; Kamiya, K.; Nakanishi, S.; Hashimoto, K. Nitrogen-doped carbon nanomaterials as non-metal electrocatalysts for water oxidation. *Nat. Commun.* **2013**, 4, 2390.

(11) Liu, Z.; Yu, X.; Yu, H.; Xue, H.; Feng, L. Nanostructured $FeNi_3$ incorporated with carbon doped with multiple nonmetal elements for the oxygen evolution reaction. *ChemSusChem*. **2018**, 11, 2703–2709.

(12) Fu, C.; Wang, Y.; Huang, J. Hybrid of quaternary layered double hydroxides and carbon nanotubes for oxygen evolution reaction. *Chin. J. Struct. Chem.* **2020**, 39, 1807–1816.

(13) Yu, L.; Ren, Z. Systematic study of the influence of IR compensation on water electrolysis. *Mater. Today Phys.* **2020**, 14, 100253.

(14) Zhang, C.; Chen, Z.; Lian, Y.; Chen, Y.; Li, Q.; Gu, Y.; Lu, Y.; Deng, Z.; Peng, Y. Copper-based conductive metal organic framework in-situ grown on copper foam as a bifunctional electrocatalyst. *Acta Phys. -Chim. Sin.* **2019**, 35, 1404–1411.

(15) Chen, X.; Zhang, Q.; Wu, L.; Shen, L.; Fu, H.; Luo, J.; Li, X.; Lei, J.; Luo, H.; Li, N. Regulation of the electronic structure of Co_4N with novel Nb to form hierarchical porous nanosheets for electrocatalytic overall water splitting. *Mater. Today Phys.* **2020**, 15, 100268.

(16) Li, M.; Liu, H.; Feng, L. Fluoridation-induced high-performance catalysts for the oxygen evolution reaction: a mini review. *Electrochem. Commun.* **2021**, 122, 106901.

(17) Yang, L.; Liu, Z.; Zhu, S.; Feng, L.; Xing, W. Ni-based layered double hydroxide catalysts for oxygen evolution reaction. *Mater. Today Phys.* **2021**, 16, 100292.

(18) Lu, H.; He, X.; Yin, F.; Li, G. Preparations of nickel-iron hydroxide/sulfide and their electrocatalytic performances for overall water splitting. *J. Electrochem.* **2020**, 26, 136–147.

(19) Sivanantham, A.; Shanmugam, S. Nickel selenide supported on nickel foam as an efficient and durable non-precious electrocatalyst for the alkaline water electrolysis. *Appl. Catal., B* **2017**, 203, 485–493.

(20) Song, S.; Yu, L.; Xiao, X.; Qin, Z.; Zhang, W.; Wang, D.; Bao, J.; Zhou, H.; Zhang, Q.; Chen, S.; Ren, Z. Outstanding oxygen evolution reaction performance of nickel iron selenide/stainless steel mat for water electrolysis. *Mater. Today Phys.* **2020**, 13, 100216.

(21) Xia, X.; Wang, L.; Sui, N.; Colvin, V. L.; Yu, W. W. Recent progress in transition metal selenide electrocatalysts for water splitting. *Nanoscale* **2020**, 12, 12249–12262.

(22) Wan, S.; Jin, W.; Guo, X.; Mao, J.; Zheng, L.; Zhao, J.; Zhang, J.; Liu, H.; Tang, C. Self-templating construction of porous $CoSe_2$ nanosheet arrays as efficient bifunctional electrocatalysts for overall water splitting. *ACS Sustainable Chem. Eng.* **2018**, 6, 15374–15382.

(23) Guo, Y.; Zhang, C.; Zhang, J.; Dastafkan, K.; Wang, K.; Zhao, C.; Shi, Z. Metal-organic framework-derived bimetallic NiFe selenide electrocatalysts with multiple phases for efficient oxygen evolution reaction. *ACS Sustainable Chem. Eng.* **2021**, 9, 2047–2056.

(24) Zhao, S.; Jin, R.; Abroshan, H.; Zeng, C.; Zhang, H.; House, S. D.; Gottlieb, E.; Kim, H. J.; Yang, J. C.; Jin, R. Gold nanoclusters promote electrocatalytic water oxidation at the nanocluster/$CoSe_2$ interface. *J. Am. Chem. Soc.* **2017**, 139, 1077–1080.

(25) Tian, Y.; Xue, X.; Gu, Y.; Yang, Z.; Hong, G.; Wang, C. Electrodeposition of Ni_3Se_2/$MoSe_x$ as a bifunctional electrocatalyst towards highly-efficient overall water splitting. *Nanoscale* **2020**, 12, 23125–23133.

(26) Zhu, H.; Jiang, R.; Chen, X.; Chen, Y.; Wang, L. 3D nickel-cobalt diselenide nanonetwork for highly efficient oxygen evolution. *Sci. Bull.*

DOI: 10.14102/j.cnki.0254-5861.2021-0037

2017, 62, 1373–1379.

(27) Liu, H.; Zha, M.; Liu, Z.; Tian, J.; Hu, G.; Feng, L. Synergistically boosting the oxygen evolution reaction of an Fe-MOF via Ni doping and fluorination. *Chem. Commun.* **2020**, 56, 7889–7892.

(28) Gao, R.; Li, G.; Hu, J.; Wu, Y.; Lian, X.; Wang, D.; Zou, X. In situ electrochemical formation of NiSe/NiO_x core/shell nano-electrocatalysts for superior oxygen evolution activity. *Catal. Sci. Technol.* **2016**, 6, 8268–8275.

(29) Liu, Z.; Zhang, C.; Liu, H.; Feng, L. Efficient synergism of $NiSe_2$ nanoparticle/NiO nanosheet for energy-relevant water and urea electrocatalysis. *Appl. Catal., B* **2020**, 276, 119165.

(30) Zhang, X.; Ding, Y.; Wu, G.; Du, X. $CoSe_2$@$NiSe_2$ nanoarray as better and efficient electrocatalyst for overall water splitting. *Int. J. Hydrogen Energy* **2020**, 45, 30611–30621.

(31) Jiang, W.; Sun, J.; Lu, K.; Jiang, C.; Xu, H.; Huang, Z.; Cao, N.; Dai, F. 2D coordination polymer-derived $CoSe_2$-$NiSe_2$/CN nanosheets: the dual-phase synergistic effect and ultrathin structure to enhance the hydrogen evolution reaction. *Dalton Trans.* **2021**, 50, 9934–9941.

(32) Wan, K.; Luo, J.; Zhou, C.; Zhang, T.; Arbiol, J.; Lu, X.; Mao, B.; Zhang, X.; Fransaer, J. Hierarchical porous Ni_3S_4 with enriched high-valence Ni sites as a robust electrocatalyst for efficient oxygen evolution reaction. *Adv. Funct. Mater.* **2019**, 29, 1900315.

(33) Kwak, I. H.; Im, H. S.; Jang, D. M.; Kim, Y. W.; Park, K.; Lim, Y. R.; Cha, E. H.; Park, J. $CoSe_2$ and $NiSe_2$ nanocrystals as superior bifunctional catalysts for electrochemical and photoelectrochemical water splitting. *ACS Appl. Mater. Interfaces* **2016**, 8, 5327–5334.

(34) Zheng, X.; Han, X.; Cao, Y.; Zhang, Y.; Nordlund, D.; Wang, J.; Chou, S.; Liu, H.; Li, L.; Zhong, C.; Deng, Y.; Hu, W. Identifying dense $NiSe_2$/$CoSe_2$ heterointerfaces coupled with surface high-valence bimetallic sites for synergistically enhanced oxygen electrocatalysis. *Adv. Mater.* **2020**, 32, 2000607.

(35) Shinagawa, T.; Garcia-Esparza, A. T.; Takanabe, K. Insight on Tafel slopes from a microkinetic analysis of aqueous electrocatalysis for energy conversion. *Sci. Rep.* **2015**, 5, 13801.

(36) Li, X.; Wu, H.; Wu, Y.; Kou, Z.; Pennycook, S. J.; Wang, J. NiFe layered double-hydroxide nanosheets on a cactuslike (Ni,Co)Se_2 support for water oxidation. *ACS Appl. Nano Mater.* **2019**, 2, 325–333.

(37) Liu, Z.; Yu, X.; Xue, H.; Feng, L. A nitrogen-doped CoP nanoarray over 3D porous Co foam as an efficient bifunctional electrocatalyst for overall water splitting. *J. Mater. Chem. A* **2019**, 7, 13242–13248.

(38) Zhang, C.; Tang, B.; Gu, X.; Feng, L. Surface chemical state evaluation of $CoSe_2$ catalysts for the oxygen evolution reaction. *Chem. Commun.* **2019**, 55, 10928–10931.

(39) Wang, S.; Zhao, L.; Li, J.; Tian, X.; Wu, X.; Feng, L. High valence state of Ni and Mo synergism in NiS_2-MoS_2 hetero-nanorods catalyst with layered surface structure for urea electrocatalysis. *J. Energy Chem.* **2022**, 66, 483–492.

(40) Guo, M.; Zhou, L.; Li, Y.; Zheng, Q.; Xie, F.; Lin, D. Unique nanosheet-nanowire structured CoMnFe layered triple hydroxide arrays as self-supporting electrodes for a high-efficiency oxygen evolution reaction. *J. Mater. Chem. A* **2019**, 7, 13130–13141.

Received: November 17, 2021
Accepted: November 29, 2021
Published: January 13, 2022

DOI: 10.14102/j.cnki.0254-5861.2021-0037